Fabrication and mechanical performance of Ti_2AlN prepared by FAST/SPS

Xiaoqiang Li *, Jesus Gonzalez-Julian, Jürgen Malzbender

Forschungszentrum Jülich GmbH, Institute of Energy and Climate, 52425 Jülich, Germany

Corresponding author*: xi.li@fz-juelich.de

Abstract

Highly dense bulk Ti_2AlN with high purity was successfully fabricated at 1400 °C by Field Assisted Sintering Technology (FAST/SPS) using Ti, Al, TiN as starting powders. Aluminum content appears to play a determinant role to attain high phase purity, where the optimum content has been achieved for a starting molar composition of 1:1.02:1 for Ti, Al, and TiN, respectively. Elastic modulus and hardness were determined via micro-indentation testing at room temperature. Regarding abrasive behavior, sandblasting tests with compressed air of 2 bar were carried out. In addition, creep tests in air in the temperature range of 900-1200 °C were performed to characterize the steady state deformation behavior under constant applied stresses ranging from 20-100 MPa.

Keywords: MAX phase; Ti_2AlN; FAST/SPS; sandblasting; creep

1. Introduction

The term '$M_{n+1}AX_n$ phase' was used for the first time by Barsoum in 2000 [1] to refer to some ternary carbides and nitrides, where "M" is an early transition element, A represents elements of group IIIA to VIA and "X" corresponds to either C or N [2-3]. All the MAX phases, at the moment more than 70 different compositions, present a hexagonal crystal structure where M_6X octahedrals are interleaved with A-A layers [4]. As a result, metallic and covalent/ionic bondings coexist in the chemical structure, exhibiting a unique combination of properties [5]. As ceramics, MAX phases possess low density, high elastic modulus, and some of them excellent oxidation and corrosion resistance at high temperature [4], meanwhile in terms of their metallic character they show high electrical and thermal conductivities, good thermal shock resistance and damage tolerance, as well as good machinability [4]. Due to their unique combination of properties listed above, MAX phases have attracted a lot of attention in the last years [2].

Among all compositions, aluminum based MAX phases appear to present the highest potential due to their excellent oxidation and corrosion resistance at high temperature related to the in-situ formation of an external, protective and well-adhered α-Al_2O_3 layer [6]. Ti_2AlC, Ti_3AlC_2 and Cr_2AlC have been the most studied MAX phases due to their excellent oxidation resistance under aggressive environmental conditions at temperature between 1000 and 1300 °C [7-9]. However, Ti_2AlN exhibits also an excellent combination of properties making it suitable for high temperature applications [10-12], despite this MAX phase has been less explored.

Compared to the rather widely studied Ti_2AlC [13-18], the mechanical properties of Ti_2AlN appear to be superior, which might be due to the fact that N contains one more valence electron than C. It enhances the chemical bonding strength and thereby also the apparent elastic modulus of Ti_2AlN compared to Ti_2AlC [19-20]. Hence, Ti_2AlN ceramics might possess more potential as structural material for high temperature applications [21-24]. Moreover, Ti_2AlN can also survive without oxidation damage up to 1200 °C and will potentially be tougher below 1200 °C [25-26]. Hence, Ti_2AlN can be considered as an excellent and promising candidate for application as structural material to be operated under aggressive environments, considering all the outstanding performance criteria reported in the literature.

Currently, bulk Ti_2AlN ceramics are mainly fabricated via hot pressing [27-31], spark plasma sintering [19,32-35], hot isostatic pressing (HIP) [36], shock-activated reaction synthesis [37] and microwave sintering [38] based on Ti/Al/TiN or Ti/AlN powder mixtures. Microstructural stability and mechanical integrity are determinant requirements to ensure the long-term reliability and stability under harsh service conditions [39-40]. At the same time, the mechanical response is also relevant in terms of scratch resistance and erosive behavior of the materials [41]. In this context, the sandblasting experiment is an application-relevant test that displays the importance of the basic mechanical properties of the investigated materials and the potential of Ti_2AlN bulk materials for the application which require abrasive resistance. Despite of its importance, sandblasting experiments have not been reported yet for MAX phase to the best knowledge of the authors.

Furthermore, one of the most important thermomechanical performance characteristics at elevated temperatures is the creep resistance of such structural materials under constant loads, which quantifies the permanent deformation and ultimately damage [42-45]. Hence, it is important to characterize and give guidelines for the improvement of the creep resistance. Works reporting creep resistance and mechanisms for MAX phases are very limited [45-50]. Furthermore, all these works refer to carbide MAX phases, whereas there are currently no publications to the best knowledge of the authors with respect to the creep behavior of nitride MAX phase materials (Ti_2AlN, Ti_4AlN_3 and so on).

Mostly, tensile creep tests were performed on fine-grain (FG) Ti_3SiC_2 ceramic within the temperature range from 1000 to 1200 °C under applied stresses of 10 to 100 MPa and the deformation mechanism was a combination of plastic deformation, crack formation and cavitation. It was verified in the respective work that plastic deformation is the dominant deformation mechanism in the steady state creep regime [45]. Furthermore, tensile creep tests were also carried out on coarse-grain (CG) Ti_3SiC_2 ceramic to study the difference of tensile creep between FG and CG Ti_3SiC_2 ceramics, in terms of the results, it appeared that the creep parameters regarding activation energy (Q) and stress exponent (n) for the tensile creep of CG and FG Ti_3SiC_2 were comparable, thus the processes responsible for the tensile creep of CG and FG Ti_3SiC_2 appeared to be the same. The compressive creep performance of hot isostatic pressed FG and CG Ti_3SiC_2 in the 1100-1300 °C temperature range was also studied [47]. At lower stresses and/or temperatures, the creep rates were a weak function of grain size. In this regime, creep rates in compression were roughly an order of magnitude lower than those in tension. The main creep mechanism was dislocation creep with possibly some grain boundary sliding. At higher stresses and/or temperatures, the stress exponents of the FG samples increase dramatically, suggesting a change of mechanism from dislocation creep to possibly sub-critical crack growth [47].

With respect to Ti_2AlC, Tallman et al. studied the tensile creep in the temperature range 1000-1150 °C for the stress range 10-40 MPa, where it was found that the parameters of tensile creep of Ti_2AlC are comparable to those of Ti_3SiC_2 [48]. Subsequent tensile creep tests performed on Ti_3AlC_2 specimens at 900 °C and 1000 °C demonstrated that deformation mechanisms at 1000 °C were the same as the ones at 900°C (140 MPa) and the creep deformation was controlled by grain boundary sliding [49]. Recently, Araki et al. [50] investigated the creep behavior of dense (2% of porosity) and porous Cr_2AlC (53% and 75%) in the temperature range of 1073-1473 K during heating and subsequent cooling after high temperature exposure for an applied stress range of 1-12 MPa. Creep appeared to be controlled by dislocation motion and/or grain boundary sliding similar as in the case of Ti_3SiC_2 [50]. In summary, it is important and hence necessary to clarify the creep behavior and mechanisms of the MAX phase materials, especially for nitride MAX phase materials.

The aim of the current work is to optimize parameters for the fabrication of the bulk Ti_2AlN ceramic with high purity, as well as the characterization of selected mechanical properties and their correlation with the microstructure. In particular, elastic modulus and micro-hardness were characterized at different loads, meanwhile the abrasion resistance was measured by sandblasting experiment using compressed air for different exposure times. Furthermore, creep resistance at elevated temperatures of dense, highly pure Ti_2AlN was characterized for the first time. The work serves as a basis for a database on the mechanical properties of this MAX phase material and also compares the properties with those of carbide and nitride MAX phase ceramics.

2. Experimental procedure

2.1 Fabrication of Ti_2AlN via FAST/SPS

Titanium (99.5 % pure), aluminum (99.5 % pure) and titanium nitride (99.5 % pure) powders (all from Alfa Aesar, Germany) were used as the starting powders. The powders were weighted according to the formula of Ti: xAl: TiN (x = 1.0, 1.01, 1.02, 1.03), and the corresponding samples were designated as Ax. The powders were mixed via Roller bench for 24 h at 250 r.p.m and using ethanol as liquid media. After the ball mixing, the slurry was dried at 60 °C in an oven for 2 days.

Ti_2AlN materials were synthesized and sintered in one step via Field Assisted Sintering Technology/Spark plasma sintering (FAST/SPS) (FCT-HPD5, FCT Systeme GmbH, Germany). The mixed powders were poured into a graphite die with an inner diameter of 20 mm and pre-compacted under uniaxial pressure of 30 MPa for 60 s. The thermal cycle was performed at different heating rates and pressures. First, a heating rate of 20 K/min with a pressure of 20 MPa from room temperature to 1000 °C was used, followed by a heating rate of 50 K/min and a pressure of 40 MPa from 1000 °C to 1400 °C. Dwell times of 15 min or 30 min were used, and the final specimens were named as Ax-15 and Ax-30, respectively.

Before characterization, the surfaces of the sintered samples were ground with 400-4000-grid SiC sandpaper to remove the layer contaminated by the graphite foil during the FAST/SPS procedure. The densities were measured by the Archimedes principle in water at room temperature. The phase compositions and the amount of different phases within the bulk materials were identified by X-ray Diffraction (XRD, D8-Discover, Bruker, US) and Rietveld refinement on the polished surfaces. The microstructure and grain distribution were characterized by field emission scanning electron microscopy (FE-SEM; Zeiss Merlin).

The samples were cut and embedded in water-free epoxy resin, then grinded with SiC sandpaper and polished with 3 μm, and subsequently 1 μm diamond polishing compound (MetaDi, BUEHLER) with colloidal silica suspension (50 nm Alkaline, CLOEREN TECGNOLOGY GmbH).

2.2 Micro-indentation

Indentation tests were conducted using a Fischerscope H100C (Helmut Fischer KG, Sindelfingen) with a Vickers tip. Various loads (10, 50, 100, 300, 500, 700, 1000 mN) were applied to characterize elastic modulus (E) and hardness (H) of the bulk Ti_2AlN ceramics. At each load, at least 64 indentations were performed to get a representative average and standard deviation. Dwelling time and acquisition rate during the tests were 5 s and 10 Hz, respectively. The E and H as a function of load of Ti_2AlN bulk material will be presented below to assess potential variabilities in these mechanical characteristics. They were evaluated based on the Oliver and Pharr methodology from the indentation load-displacement curve [51], see also [52-53], considering a Poisson's ratio (v) of 0.20 for Ti_2AlN [54-55].

2.3 Sandblasting test

In order to investigate the abrasive resistance of Ti_2AlN, a test series was carried out using a sandblasting machine MHG BNP 210 (MHG Strahlanlagen GmbH, Düsseldorf). Details on the setup can be found in [41]. Briefly, the bulk Ti_2AlN ceramics were cut into discs with a diameter of 25 mm and thickness of 2.5 mm. A special sample holder was designed to fix the samples at a constant distance and an angle of 45° to the beam. Magnetic holders were used to fix the sample to the bottom of the sandblasting box. To ensure the constant beam alignment, the sand blasting pistol was also fixed. The glass beads were used as the grid to blast the surface with pressurized air (2 bar), obtained from MHG, with an average grain diameter of 150-250 μm [56]. After testing for 1 min, the tested sample were taken out from the holder and weighed with a precision balance Mettler-Toledo XS205 Dualrange (Mettler-Toledo GmbH, Gieβen) with a measuring accuracy of 0.01 mg to calculate the mass loss.

2.4 Compressive creep tests

Ti_2AlN samples were cut by electrical discharge machining into cylindrical specimens with the dimension diameter 6.0-6.5 mm and height of about 8.0 mm. Similar as in [42-44, 57] the steady-stage creep rates were obtained via long-term compression tests at different temperatures and applied stresses, using an

Instron 1362 electromechanical testing machine, equipped with a high temperature furnace. First, the cylindrical Ti_2AlN specimens were mounted between a half-sphere (top) and Al_2O_3 plate (bottom) with a coating of BN via the BN spraying agent (Boron Nitride Grade TG, 3M Technical ceramics) on the surfaces of plates to avoid the reactions between Ti_2AlN and alumina during the high temperature test. Second, the specimens were preloaded with a compressive force of 2 N to fix them. Third, a heating with a rate of 5 K/min was applied to reach the target temperature. To reach equilibrium conditions, the test specimens were heated up to the target temperature with the heating rate of 5 K/min and the temperature was held for 1 h before creep test. In order to measure the displacement during the test, a linear variable differential transformer (Solartron Metrology) with alumina coupling rods was utilized over the whole time. The compressive creep tests were carried out in air from 900 °C to 1200 °C (maximum temperature limited to avoid excessive oxidation of the specimens) under different constant loads corresponding to stress levels of 20-100 MPa, the creep tests were terminated when the steady-state deformation was confirmed or until an integral deformation of 100 μm was reached. The conditions of the creep test on A1.02-15 are listed in Table 1.

After a short primary creep stage, the deformation rate typically reduces rapidly. The subsequent steady state creep rate in the secondary stage (simply called "creep rate" hereafter) is thermally activated, known to depend on temperature T and stress σ, and can be described by the following equation [46, 50]:

$$\dot{\varepsilon} = \dot{\varepsilon}_0 A\left(\frac{\sigma}{\sigma_0}\right)^n exp\left(-\frac{Q}{RT}\right) \qquad (1)$$

Where A, n, Q, and R are the stress-independent constant (Dorn constant), stress exponent, activation energy for creep, and gas constant, respectively. $\dot{\varepsilon}_0$ and σ_0 are 1 s^{-1} and 1 MPa, separately, used for defining the dimensions of strain rate and stress.

The creep rate was determined from the slope in the secondary stage via a linear fitting regression. The slope of straight lines plotted by fitting the data of minimum creep rate with respect to inverse of absolute temperature and ln of the applied stress gives the activation energy and stress exponent respectively. Eq. (1) is simplified into a linear equation (y= ax + b) by applying the natural logarithm on both sides of the equation where A accounts for the slope of the fitted line. The tests were aborted before reaching the tertiary creep regime.

3. Results and discussion

Fig. 1 presents the representative sintering curve of A1.02-15 prepared via FAST/SPS, the displacement increased with the increasing sintering time. As reported also in literature [19, 32], the whole sintering curve during the FAST/SPS can be separated into following stages: 1) The arrangement and compaction of the raw powder mixture from room temperature to 500 °C, resulting from heating and application of load, are the main factors for the densification. 2) The melting of aluminum and the reactions to form intermetallic phases lead to a rapid increase of displacement in the temperature range 500-600 °C. 3) The displacement curve ranging from 600 °C to 900 °C is very flat and stable, which can be attributed to the slightly different products and no more new phases being created that might change the volume within this temperature range. 4) The strong variation of the densification displacement within the temperature range of 900-1200 °C indicates that the formation of Ti_2AlN phase and densification mainly occurs within this temperature range because of the high temperature and applied load. 5) The slight increase of the displacement above 1200 °C can be associated with the removal of small pores and further reactions

consuming the remaining intermetallics. Finally, after the process the Ti_2AlN ceramic is almost fully dense, since the displacement is almost stable after a dwelling time of 10 min at 1400 °C.

Fig. 2(a) shows the XRD patterns of the sintered bulk Ti_2AlN samples as a function of the aluminum content. As shown in Fig. 2(a), almost all diffraction peaks correspond to those of pure Ti_2AlN. However, the magnified range from 35° to 45° shown in Fig. 2(b), clearly reveals that some impurities exist in some of the derived Ti_2AlN ceramics, such as Ti_3Al etc. Therefore, as might be expected, aluminum plays a determinant role in the synthesis of Ti_2AlN due to its low melting point and the possible evaporation during the sintering. In order to investigate the influence of aluminum content on the purity in more detail, the obtained bulk Ti_2AlN compositions were characterized via Rietveld analysis as shown in Fig. 3 and Table 2. The lattice parameters of Ti_2AlN calculated via Rietveld refinement are $a^* = b^* = 2.987$ Å, $c^* = 13.645$ Å, which agree well with the previous data reported by Barsoum et al. ($a^* = b^* = 2.989$ Å and $c^* = 1.3614$ Å) [3] and Lin et al ($a^* = b^* = 2.990$ Å and $c^* = 1.3620$ Å) [19].

Considering the data in Fig. 3 and Table 2, A1.02-15 has no detectable impurities, implying the highest purity for an excess Al content of 2 at.%. As shown in Fig. 2 (a), the identification is rendered highly difficult since the concentration of the impurities is low and peaks overlap with the Ti_2AlN peaks. Therefore, in order to illustrate the reliability of the calculated results, the difference between the calculated and the detected signals of A1.02-15 is as illustrated in Fig. 4 small, revealing the reliability of high purity for A1.02-15.

Based on all above, the amount of aluminum plays a very significant role in the improvement of purity and hence a small additional amount of aluminum powder was added to compensate the Al loss during the fabrication procedure [9, 58], while any further excess of aluminum will also result in the occurrence of some impurities, such as the TiAl intermetallic (TiAl, Ti_3Al etc.).

The density of A1.02-15 is 4.307 g/cm^3 (theoretical density is 4.31 g/cm^3 [3, 19, 59]), yielding an experimental over theoretical density ratio higher than 99 % and offering the possibility to test the mechanical performance of a dense Ti_2AlN ceramic without any significant detrimental influence of pores.

Furthermore, in order to check the impact of the dwelling time on grain size and thermal stability of Ti_2AlN, the A1.02 powder was additionally sintered with a holding time of 30 min under the same parameters of heating rate and pressure. As shown in Table 2, the resulting A1.02-30 samples were thermally stable without decomposition effects as confirmed also for A1.02-15.

Overall, the A1.02 powder appeared to be the most appropriate one compared to other compositions in the current work. Hence, the focus of further investigations was directed towards specimens A1.02-15 and A1.02-30 regarding microstructural observations and mechanical testing considering their high purity.

To characterize the microstructural morphology and phase compositions of the sintered samples, back-scattered electron images were acquired. These BSE images and associated EDS results of polished surfaces for the bulk Ti_2AlN ceramics sintered at 1400 °C are shown in Fig. 5, which confirms the high density of the material. Nevertheless, some impurity Al_2O_3 particles (point 2) are homogenously distributed within the Ti_2AlN ceramic. The raw aluminum powder presumably oxidized to Al_2O_3 by oxygen traces in the starting precursors during the storage of raw materials and the drying of the powder mixture in the oven.

In order to investigate the impact of the dwelling time on the grain size, SEM images of fracture surfaces were obtained (Figure 6). An uniform, equiaxed morphology of Ti_2AlN grains was detected and their

layered-grain structure character is evident. The grain size of A1.02-30 is slightly larger than that of A1.02-15. The grain sizes of A1.02-15 and A1.02-30 are calculated to be 10 ± 5 μm and 13 ± 7 μm, respectively, based on the EBSD images shown in Fig. 7. The A1.02-30 has some abnormally large Ti_2AlN grains with grain sizes ranging from 35 to 55 μm, which is not observed for A1.02-15, presumably due to the shorter dwelling time. The yellow indicated phase corresponds to Al_2O_3 particles, meanwhile the red grains correspond to Ti_2AlN phase.

Elastic modulus and hardness as a function of applied load (corresponding to an increase in indentation depth) are shown in Fig. 8. The elastic moduli of A1.02-15 and A1.02-30 are almost constant, however *H* decreases slightly with increasing load, being especially visible above 500 mN, which might be related to a larger contribution of grain boundaries [60], perhaps also to the widely reported indentation size effect [61-64]. The elastic moduli and hardness values for the load range of 50 mN to 1000 mN of A1.02-15 are 252 ± 19 GPa and 7-11 GPa, respectively, and those of A1.02-30 are 254 ± 19 GPa and 7-10 GPa, respectively, hence, elastic moduli of A1.02-15 and A1.02-30 are almost the same, note, normally this property is independent on the grain size. In contrast, on the basis of the Hall–Petch relationship, which is the basis of the indentation size effect, the hardness of A1.02-15 might be expected to be higher than that of A1.02-30 due to finer grain of A1.02-15, although such a difference is not obvious from the results.

As reported, the elastic modulus of Ti_2AlN is ~ 286 GPa experimentally determined by impulse excitation technique [19] and 293 GPa based on calculation [65], which are both higher than the values derived from micro-indentation test. The difference might be related to surface roughness effects [66] and furthermore, differences due to polycrystalline samples and various additional factors, such as local porosity and grain boundaries, could affect the testing result.

To study the abrasion resistance of Ti_2AlN, the mass losses obtained after sandblasting tests are compared in Fig. 9. As might be expected, the mass losses of A1.02-15 and A1.02-30 reveal a similar tendency. After exposure for about 10 min, the mass losses of A1.02-15 and A1.02-30 reach 0.73 wt.% and 0.66 wt.%, respectively. Hence, A1.02-30 displays a slightly smaller mass loss than A1.02-15, which might be attributed to the larger grain size of A1.02-30. Note, being out of the scope of the current investigation, a deeper investigation will be conducted in future works.

Regarding the compressive creep tests of the bulk Ti_2AlN ceramics, as outlined above, A1.02-15 appears to be the most suitable candidate in the current work, hence this composition was selected for the creep tests. Moreover, the grain size of A1.02-15 is comparable to those of other specimens used in reported creep test on other MAX phase ceramics, such as 3-5 μm for Ti_3SiC_2 [45, 47], 14 ± 8 μm for Ti_2AlC ceramic [48], 4.9-12.5 μm for Ti_3AlC_2 ceramic [49], and ~ 9 μm for Cr_2AlC [50], permitting hence a more straightforward comparison with previous investigations on carbide MAX phase ceramics.

An example of a creep deformation curve for 1000 °C under 60 MPa is shown in Fig. 10. The specimen shows a relatively large deformation under these conditions, and the curve reveals two stages: (i) primary creep regime with a rapidly decreasing creep rate also known as transient creep stage, (ii) secondary creep regime (steady state creep) with a constant creep rate.

Fig. 11 presents an Arrhenius plot of the creep rate of A1.02-15 versus the reciprocal absolute temperature for the temperature range of 900 °C to 1200 °C in air under constant stresses ranging from 20 MPa to 100 MPa. As expected, the creep rates increases at higher stresses and testing temperatures. The creep activation energy was obtained via global linear fitting of all results using the software “Origin”. Obviously, the quality of the individual data description by the global linear fitting is very similar and the derived activation energy of the FAST/SPS prepared Ti_2AlN is calculated to be 274 ± 7 kJ/mol.

Fig. 12 shows the ln-ln plots of creep rates as a function of applied stress for the temperature ranging from 900-1200 °C. Global linear fitting regression was applied to obtain the stress exponent (n), since the slopes of the individual plots at different temperatures are very similar. The stress exponent (n) is calculated to be 1.2 ± 0.1. As might be expected, there is no temperature dependency of the stress exponent for the bulk Ti_2AlN ceramic.

Until now, there are only a few studies on the creep behavior of MAX phase ceramics. For example, creep tests on Ti_3SiC_2 ceramic with fine grain size of 3-5 μm under tension and compression in the temperature range of 1000-1200 °C and stress level of 10-100 MPa yielded values of Q and n of 445-537 kJ/mol and 1.5-1.9, respectively. Dislocation creep was proposed to be the dominant mechanism in the secondary creep regime [45-47]. The creep behavior of dense Ti_2AlC was also investigated yielding for Q and n of 362 kJ/mol and 2.5, respectively, and dislocation creep with possibly grain boundary sliding was proposed as the dominant creep mechanism [48]. For the creep test of dense Ti_3AlC_2, the parameter n was 2.34-2.50, and it was reported that creep mechanism of Ti_3AlC_2 at 900 °C was controlled by grain boundary sliding [49]. Recently, compressive creep tests were carried out for dense Cr_2AlC, and the resulting parameters of Q and n were 429 ± 13 kJ/mol and 2.7 ± 0.2, respectively, and it was suggested that in this case the dominant creep mechanism was supposed to be dislocation motion [50]. All the results of the previous reports about the creep test on MAX phase ceramics along with those obtained in current work are summarized in Table 3.

Since the creep parameters of Ti_2AlN, obtained in the current study are overall comparable with the reported results on the other MAX phase materials, the creep behavior of dense Ti_2AlN may be also controlled by the dislocation motion and/or the grain boundary sliding and more investigations will be carried out to have a deeper understanding regarding the creep mechanism of Ti_2AlN ceramics and MAX phase ceramics in our further work.

4. Conclusion

Optimized parameters for the fabrication of bulk Ti_2AlN ceramics via FAST/SPS sintering were derived and highly dense bulk Ti_2AlN ceramics with high purity were successfully fabricated at 1400 °C with different dwelling times using Ti, Al, TiN as starting powder with the Al molar ratio of 1.02. The elastic modulus and hardness were determined via micro-indentation. The elastic moduli and hardness of bulk Ti_2AlN ceramics with the initial Al ratio of 1.02 sintered with 15 min (A1.02-15) and 30 min (A1.02-30) are 252 ± 19 and 7-11 GPa, 254 ± 19 and 7-10 GPa, respectively, hence for both variants rather similar. Both bulk Ti_2AlN ceramics present similar mechanical performance, indicating both of them have great potential as excellent structural materials in the future. In addition, the abrasive resistance of Ti_2AlN was determined by sandblasting test with compressed air of 2 bar. After the exposure of the sandblasting for 10 min, the mass losses of A1.02-15 and A1.02-30 reached 0.73 wt.% and 0.66 wt.%, respectively. Initial creep tests in air in the temperature range of 900-1200 °C on bulk Ti_2AlN ceramic were conducted to characterize the deformation behavior under constant stresses ranging from 20-100 MPa. The creep parameters of Ti_2AlN, obtained in the current study, are overall comparable with the results on the other carbide MAX phases, thus, the creep behavior of dense Ti_2AlN may be controlled by the dislocation motion and/or the grain boundary sliding where more investigations are needed in future to clarify the creep mechanism.

Acknowledgements

The authors would like to thank Mr. R. Steinert for technical support of FAST/SPS, Mr. M. Turiaux for the support the creep tests, Dr. E. Wessel, Dr. D. Grüner for microstructural investigation via SEM, and Mr. M. Ziegner for the supporting the work with XRD investigations. Supports from Prof. Dr. L. Singheiser and Prof. M. Krüger are highly acknowledged. Mr. X. Li gratefully acknowledge the support from the China Scholarship Council of China. Prof. Dr. J. Gonzalez-Julian thanks the financial support by the Germany's Federal Ministry of Education and Research ("Bundesministerium für Bildung und Forschung") under the MAXCOM project (03SF0534).

References

[1] M.W. Barsoum, The $M_{n+1}AX_n$ phases: a new class of solids; thermo-dynamically stable nanolaminates, Prog. Solid. State. Chem. 28 (2000) 201-281.

[2] Y. Bai, N. Srikanth, C.K. Chua, K. Zhou, Density Functional Theory Study of $M_{n+1}AX_n$ Phases: A Review, Crit. Rev. Solid. State. 44 (1) (2019) 56-107.

[3] M.W. Barsoum, M. Radovic, Elastic and Mechanical Properties of the MAX Phases, Annu. Rev. Mater. Res. 41 (2011) 195-227.

[4] Z.M. Sun, Progress in research and development on MAX phases: a family of layered ternary compounds, Int. Mater. Rev. 56 (3) (2011) 143-166.

[5] Z.M. Sun, Y.C. Zhou, The electronic structure and chemical bonding of Ti_3GeC_2, J. Mater. Chem. 10 (2) (2000) 343-345.

[6] A.S. Farle, C. Kwakernaak, S. van der Zwaag, W.G. Sloof, A conceptual study into the potential of $M_{n+1}AX_n$-phase ceramics for self-healing of crack damage, J. Eur. Ceram. Soc. 35 (1) (2015) 37-45.

[7] D.J. Tallman, B. Anasori, M.W. Barsoum, A critical review of the oxidation of Ti_2AlC, Ti_3AlC_2 and Cr_2AlC in air, Mater. Res. Lett. 1 (2013) 115-125.

[8] J. Gonzalez-Julian, T. Go, D.E. Mack, R. Vaßen, Environmental resistance of Cr_2AlC MAX phase under thermal gradient loading using a burner rig. J. Am. Ceram. Soc. 101 (5) (2018) 1841-1846.

[9] J. Gonzalez-Julian, S. Onrubia, M. Bram, C. Broeckmann, R. Vassen, O. Guillon, High-temperature oxidation and compressive strength of Cr_2AlC MAX phase foams with controlled porosity, J. Am. Ceram. Soc. 101 (2018) 542-552.

[10] M. Undberg, K. Lindgren, El-Raghy. T, G. Malmqvist, US Patent 10, 544, 467; 2004.

[11] T. El-Raghy, M.W. Barsoum, US Patent 10, 666, 639; 2003.

[12] J.Y. Li, Y.Y. Cui, R. Yang, US Patent 11, 629, 559; 2005.

[13] X.H. Wang, Y.C. Zhou, Solid-Liquid Reaction Synthesis and Simultaneous Densification of Polycrystalline Ti_2AlC, Z. Metallkd. 93 (1) (2002) 66-71.

[14] Y.C. Zhou, Z.M. Sun, Electronic structure and bonding properties of layered machinable Ti_2AlC and Ti_2AlN ceramics, Phys. Rev B. 61 (19) (2000) 75120-12573.

[15] W.B. Zhou, B.C. Mei, J. Q. Zhu, X.L Hong, Rapid synthesis of Ti_2AlC by spark plasma sintering technique, Mater. Lett. 59 (1) (2005) 131-134.

[16] G. Hug, E. Fries, Full-potential electronic structure of Ti_2AlC and Ti_2AlN, Phys. Rev. B 65 (2002) 113104.

[17] A.G. Zhou, C.A. Wang, Z.B Ge, L.F Wu, Preparation of Ti_3AlC2 and Ti_2AlC by self-propagating high-temperature synthesis, J. Mater. Sci. Lett. 20 (2001) 1971-1973.

[18] P. Wang, B.C. Mei, X.L. Hong, W.B. Zhou, Synthesis of Ti_2AlC by hot pressing and its mechanical and electrical properties, Trans. Nonferrous. Met. Soc. China. 17 (5) (2007) 1001-1004.

[19] Z.J. Lin, M.J. Zhuo, M.S. Li, J.Y. Wang and Y.C. Zhou, Synthesis and microstructure of layered-ternary Ti_2AlN ceramic, Scr. Mater. 56 (2007) 1115-1118.

[20] Z.M. Sun, D. Music, R. Ahuja, J.M. Schneider, Ab initio study of M_2AlN (M = Ti,V, Cr), J. Phys. Condens. Matter. 17 (2005) 15-19.

[21] M. Bugnet, T. Cabioc'h, V. Mauchamp, Ph. Guérin, M. Marteau, M. Jaouen, Stability of the nitrogen-deficient Ti_2AlN_x MAX phase in Ar^{2+} irradiated (Ti,Al)N/Ti_2AlN_x multilayers, J. Mater. Sci. 45 (2010) 5547.

[22] J.Z. Duan, J.R. Zhang, C.L. Wang, Y. Qiu, W.S. Duan, L. Yang, First principles investigation of point defect-related properties in Ti_2AlN, RSC. Adv. 4 (2014) 42014-42021.

[23] E.S Choi, J.W Sung, Q. M Wang, K.H. Kim, A. Busnaina, M.C. Kang, Material properties and machining performance of hybrid Ti_2AlN bulk material for micro electrical discharge machining, Trans. Nonferrous. Met. Soc. China. 22 (3) (2012) 781-786.

[24] M.K. Drulis, H. Drulis, A.E. Hackemer, A. Ganguly, T. El-Raghy, M.W.Barsoum, On the low temperature heat capacities of Ti_2AlN and $Ti_2Al(N_{0.5}C_{0.5})$, J. Alloy. Compd. 433 (1-2) (2007) 59-62.

[25] B. Cui, R. Sa, D.D. Jayaseelan, F. Inam, M.J. Reece, W. Edward Lee, Microstructural evolution during high-temperature oxidation of spark plasma sintered Ti_2AlN ceramics, Acta. Mater 60 (2012) 1079-1092.

[26] B. Cui, W. Edward Lee, High-temperature Oxidation Behavior of MAX Phase Ceramics, Refra. Worldforum 5 (2013) 1.

[27] H. Hashimoto, Z.M. Sun, An approach to the synthesis of AlN-Ti_2AlN composite. J. Jpn. Soc. Powder. Metall. 56 (2009) 541-5.

[28] S. Lu, X.Q. Li, Y.F. Zhou , W.T. Xu, W. Pan, Synthesis and mechanical properties of TiB_2/Ti_2AlN composites fabricated by hot pressing sintering, J. Ceram. Soc. Jan. 126 (11) (2018) 900-905.

[29] C. Salvo, E. Chicardi, C. García-Garrido, J. A. Jiménez, C. Aguilar, J. Usuba, R. V. Mangalaraja, The influence of mechanical activation process on the microstructure and mechanical properties of bulk Ti_2AlN MAX phase obtained by reactive hot pressing, Ceram. Int. 45 (14) (2019) 17793-17799.

[30] I.M. Low, W.K. Pang, S.J. Kennedy, R.I. Smith, High-temperature thermal stability of Ti_2AlN and Ti_4AlN_3: A comparative diffraction study, J. Eur. Ceram. Soc. 31 (2011) 159-166.

[31] M. Yan, Y. L. Chen, B. C. Mei, Synthesis of high purity Ti_2AlN ceramic by hot pressing, Trans. Nonferrous. Met. Soc. China. 18 (1) (2008) 82-5.

[32] M. Yan, B.C. Mei, J.Q. Zhu, C.G. Tian, P. Wang, Synthesis of high-purity bulk Ti_2AlN by spark plasma sintering (SPS), Ceram. Int. 34 (2008) 1439-1442.

[33] Y. Liu, Z.Q. Shi, J.P. Wang, G.J. Qiao, Z.H. Jin, Z.J. Shen, Reactive consolidation of layered-ternary Ti_2AlN ceramics by spark plasma sintering of a Ti/AlN powder mixture, J. Eur. Ceram. Soc. 31 (2011) 863-868.

[34] Y. Liu, Y.X. Li, F. Li, H. Cui, Y.P. Pu, S.W. Guo, Z.Q. Shi, Highly textured Ti_2AlN ceramic prepared via thermal explosion followedby edge-free spark plasma sintering, Scr. Mater. 136 (2017) 55-58.

[35] V.G. Gilev, M.N. Kachenyuk, Phase Formation in the Synthesis of Ti_2AlN by Spark Plasma Sintering in the Ti/AlN System, Refract. Ind. Ceram. 59 (6) (2019) 658-662.

[36] A. Guitton , A. Joulain , L. Thilly, C, Tromas, Dislocation analysis of Ti_2AlN deformed at room temperature under confining pressure, Philos. Mag. 92 (36) (2012) 4536-4546.

[37] J.L. Jordan, N.N. Thadhani, Effect of shock-activation on post-shock reaction synthesis of ternary ceramics, AIP conference proceedings, IOP Institute of Physics Publishing Ltd. (2) (2002) 1097-1100.

[38] W.L. Liu, C.J. Qiu, J. Zhou, Z.H. Ding, X.B Zhou, S.Y. Du, Y.H. Han, Q. Huang, Fabrication of Ti_2AlN ceramics with orientation growth behavior by the microwave sintering method, J. Eur. Ceram. Soc. 35 (5) (2015) 1385-1391.

[39] V. Thomas Paul, S. Saroja, M. Vijayalakshmi, Microstructural stability of modified 9Cr-1Mo steel during long term exposures at elevated temperatures, J. Nucl. Mater. 378 (3) (2008) 273-281.

[40] M. Marrony, R. Barrera, S. Quenet, S. Ginocchio., L. Montelatici, A. Aslanides, Durability study and lifetime prediction of baseline proton exchange membrane fuel cell under severe operating conditions, J. Power. Sources. 182 (2) (2008) 469-475.

[41] S. von Helden, J. Malzbender, M. Krüger, Mechanical properties, wear resistance and surface damage of glasses and $MgAl_2O_4$ spinel ceramic after abrasion and scratch exposure, Ceram. Int. 45 (8) (2019) 10765-10775.

[42] Y. Zou, F. Schulze-Küppers, M. Balaguer, J. Malzbender, M. Krüger, Creep behavior of porous $La_{0.6}Sr_{0.4}Co_{0.2}Fe_{0.8}O_{3-\delta}$ substrate material for oxygen separation application, J. Eur. Ceram. Soc. 38 (4) (2018) 1702-1710.

[43] J. Wei, J. Malzbender, Steady state creep of Ni-8YSZ substrates for application in solid oxide fuel and electrolysis cells, J. Power. Sources. 360 (2017) 1-10.

[44] S.F.P. Ten Donkelaar, V. Stournari, J. Malzbender, A. Nijmeijer, H.J.M. Bouwmeester, High-temperature compressive creep behavior of perovskite-type oxides $SrTi_{1-x}Fe_xO_{3-\delta}$, J. Eur. Ceram. Soc. 35 (15) (2015) 4203-4209.

[45] M. Radovic, M.W. Barsoum, T. El-Raghy, S.M. Wiederhorn, Tensile creep of fine-grained (3-5 μm) Ti_3SiC_2 in the 1000-1200 °C temperature range, Acta. Mater. 49 (2001) 4103-12.

[46] M. Radovic, M.W. Barsoum, T. El-Raghy, S.M. Wiederhorn, Tensile creep of coarse-grained Ti_3SiC_2 in the 1000-1200 °C temperature range, J. Alloys. Compd. 361 (2003) 299-312.

[47] T. Zhen, M.W. Barsoum, S.R. Kalidindi, M. Radovic, Z.M. Sun, T. El-Raghy, Compressive creep of fine and coarse-grained Ti_3SiC_2 in air in the 1100–1300°C temperature range, Acta. Mater. 53 (2005) 4963-4973.

[48] D.J. Tallman, M. Naguib, B. Anasori, M.W. Barsoum, Tensile creep of Ti_2AlC in air in the temperature range 1000-1150 °C, Scr. Mater. 66 (2012) 805-808.

[49] E. Drouelle, A. Joulain, J. Cormier, V. Gauthier-Brunet, P. Villechaise, S. Dubois, P. Sallot, Deformation mechanisms during high temperature tensile creep of Ti_3AlC_2 MAX phase, J. Alloys. Compd. 693 (2017) 622-630.

[50] W. Araki, J. Gonzalez-Julian, J. Malzbender, High temperature compressive creep of dense and porous Cr_2AlC in air, J. Eur. Ceram. Soc. 39 (2019) 3660-3667.

[51] W.C. Oliver, G.M. Pharr, An improved technique for determining hardness and elastic modulus using load and displacement sensing indentation experiments, J. Mater. Res. 7 (2011) 1564-1583.

[52] J. Malzbender, Comment on hardness definitions, J. Eur. Ceram. Soc. 23 (2003) 1355-1359.

[53] T. Wakui, J. Malzbender, R.W. Steinbrech, Strain dependent stiffness of plasma sprayed thermal barrier coatings, Surf. Coat. Technol. 200 (2006) 4995-5002.

[54] W. Feng, S. Cui, Mechanical and electronic properties of Ti_2AlN and Ti_4AlN_3: a first-principles study, Can. J. Phys. 92 (12) (2014) 1652-1657.

[55] W.Y. Ching, Y. Mo, S. Aryal, P. Rulis, Intrinsic Mechanical Properties of 20 MAX-Phase Compounds, J. Am. Ceram. Soc. 96 (7) (2013) 2292-2297.

[56] https://www.mhgstrahlanlagen.de/de/strahlanlagen/strahlmittel/glaskugeln. html (2018). Data Sheet MHG glass beads Typ 207.

[57] Y. Zou, F. Schulze-Küppers, J. Malzbender, Creep behavior of porous $La_{0.6}Sr_{0.4}Co_{0.2}Fe_{0.8}O_{3-\sigma}$ oxygen transport membrane supports, Ceram. Int. 41 (3) (2015) 4064-4069.

[58] J. Gonzalez-Julian, S. Onrubia, M. Bram, O. Guillon, Effect of sintering method on the microstructure of pure Cr_2AlC MAX phase ceramics, J. Ceram. Soc. Jan. 124 (4) (2016) 415-420.

[59] D.Q. Wang, D. Li. Sun, X.L. Han, Q. Wang, G.W. Wang, Investigation on Tribological Properties of the Pre-oxidized Ti_2AlN/TiAl Composite, J. Mater. Eng. Perform. 27 (2018) 1973.

[60] J.F. Nonemacher, S. Naqash, F. Tietz, J. Malzbender, Micromechanical assessment of Al/Y-substituted NASICON solid electrolytes, Ceram. Int. 45 (17) (2019) 21308-21314.

[61] J. Gong, J. Wu, Z. Guan, Analysis of the indentation size effect on the apparent hardness for ceramics, Mater. Lett. 38 (3) (1999) 197-201.

[62] A.A. Elmustafa, D.S. Stone. Nano-indentation and the indentation size effect: Kinetics of deformation and strain gradient plasticity, J. Mech. Phys. Solids. 51 (2) (2003) 357-381.

[63] S.J. Bull, T.F. Page, E.H. Yoffe, An explanation of the indentation size effect in ceramics. Phil. Mag. Lett. 59 (6) (1989) 281-288.

[64] G.P. Bei, V. Gauthier-Brunet, C. Tromas, S. Dubois, Synthesis, Characterization, and Intrinsic Hardness of Layered Nanolaminate Ti_3AlC_2 and $Ti_3Al_{0.8}Sn_{0.2}C_2$ Solid Solution, J. Am. Ceram. Soc. 95 (1) (2012) 102-107.

[65] B. Holm, R. Ahuja, S. Li, B. Johansson, Theory of the ternary layered system Ti-Al-N, J. Appl. Phys. 91 (2002) 9874.

[66] M. S. Bobji, S. K. Biswas, Hardness of a surface containing uniformly spaced pyramidal asperities, Trib. Lett. 7 (1999) 51.

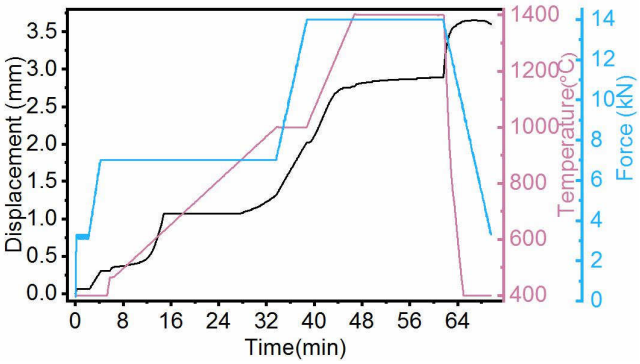

Fig.1 The representative sintering curve of A1.02-15.

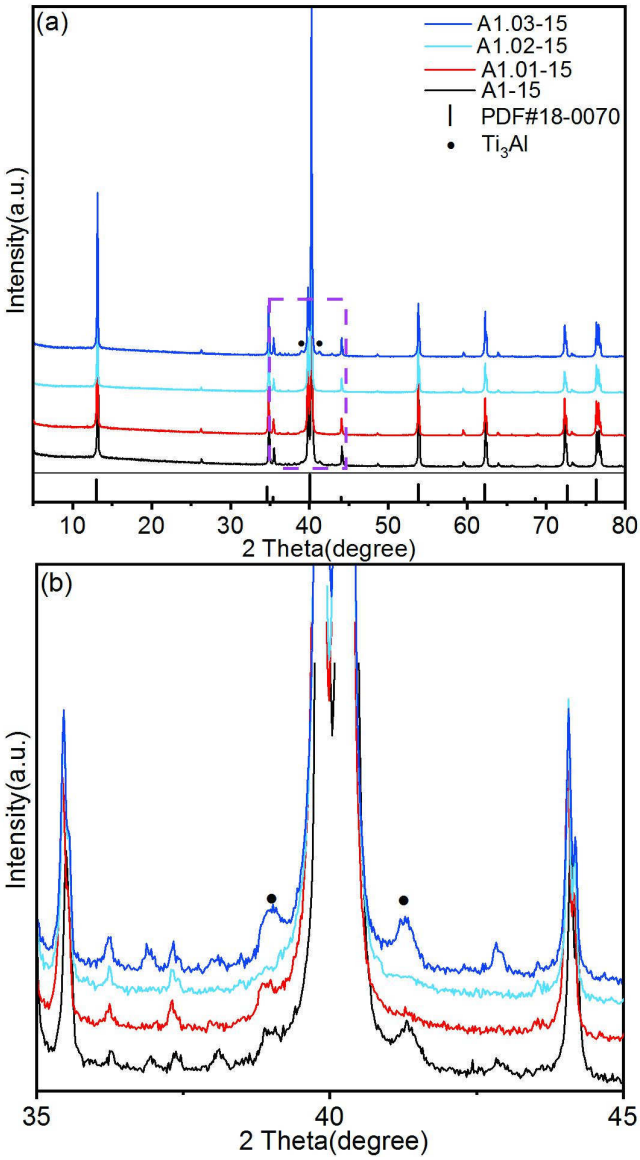

Fig.2 The XRD patterns of (a) obtained Ti_2AlN bulk material with different aluminum content; (b) the magnified range from 35 to 45°.

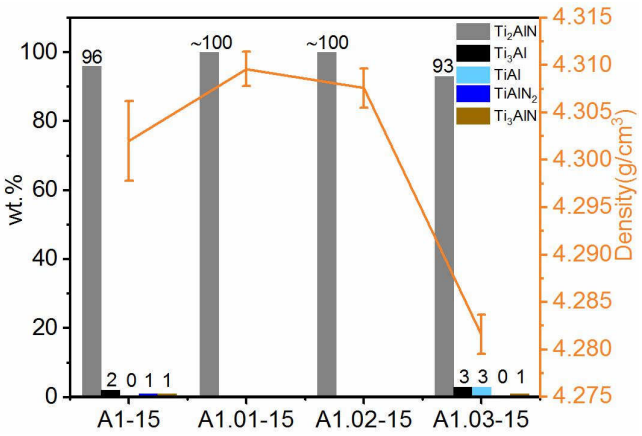

Fig.3 The amount of different phases and the densities of bulk Ti_2AlN ceramics with different Al ratio.

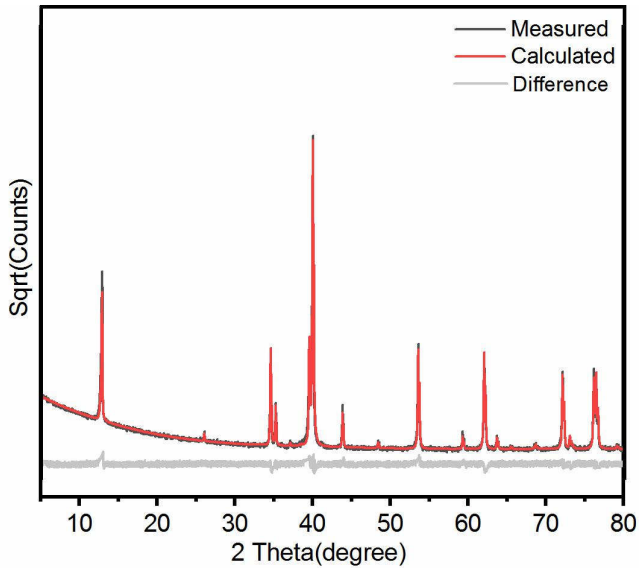

Fig.4 The Rietveld analysis of A1.02-15.

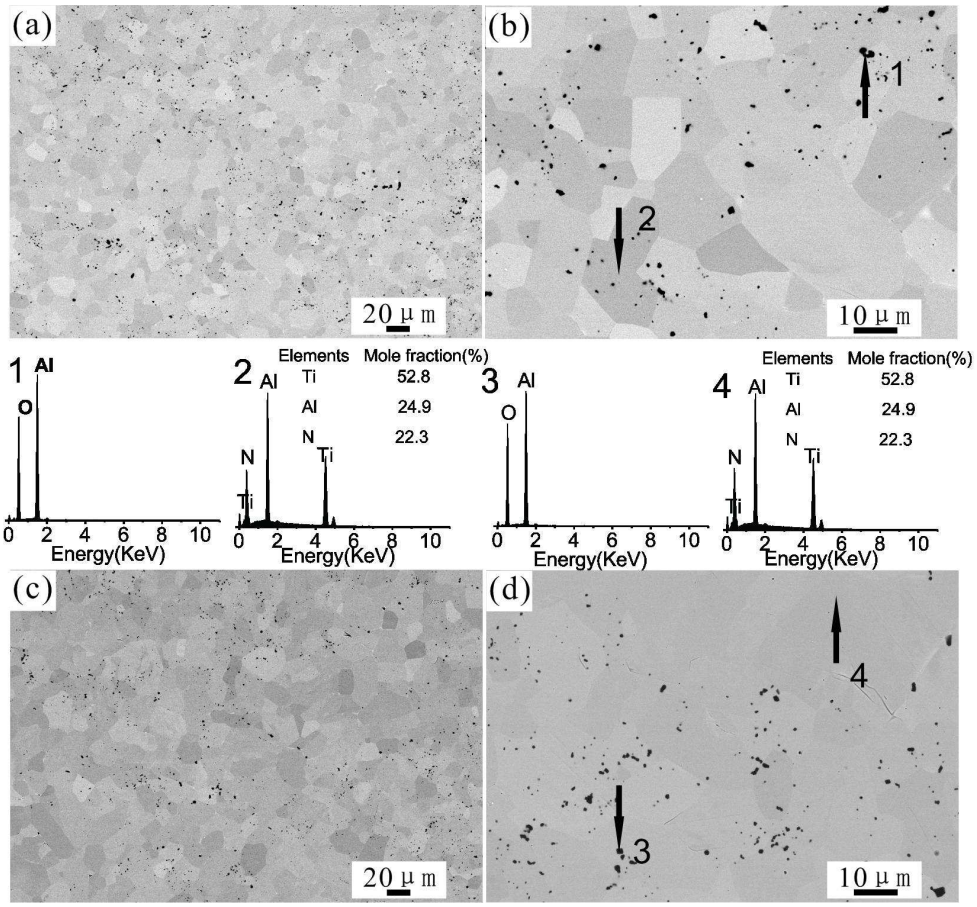

Fig.5 The SEM images of polished surfaces of FAST/SPSed Ti_2AlN, A1.02-15 in (a) low magnification; (b) high magnification; A1.02-30 in (c) low magnification; (d) high magnification and corresponding EDS results.

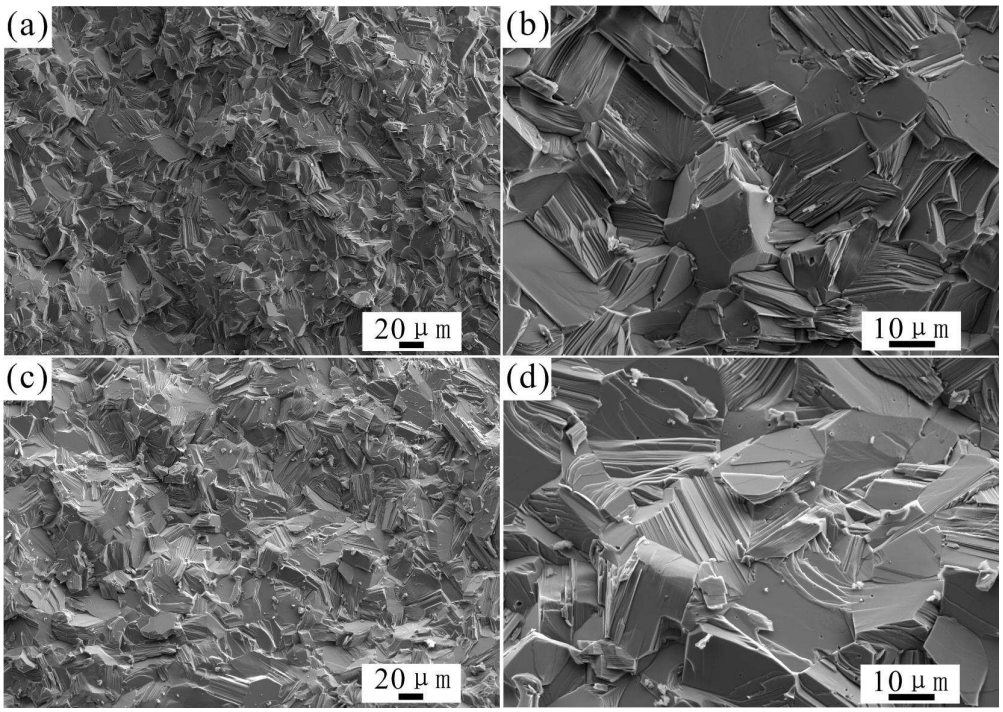

Fig.6 The SEM images of fracture surfaces of FAST/SPSed Ti_2AlN: A1.02-15 in (a) low magnification; (b) high magnification; A1.02-30 in (c) low magnification; (d) high magnification.

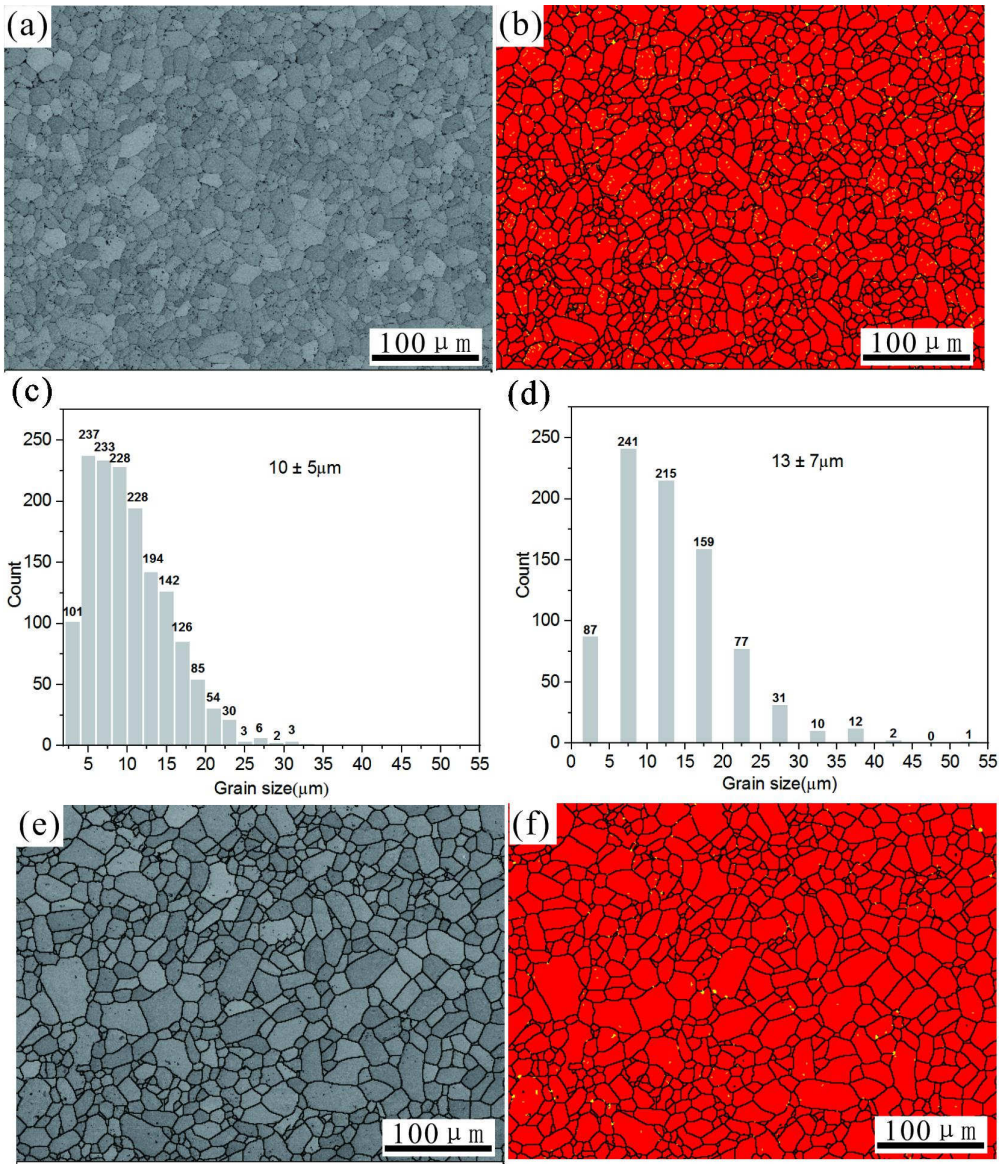

Fig.7 The phase distribution map of (a)(b)A1.02-15; (e)(f) A1.02-30 and (c)(d) corresponding grain size distribution results.

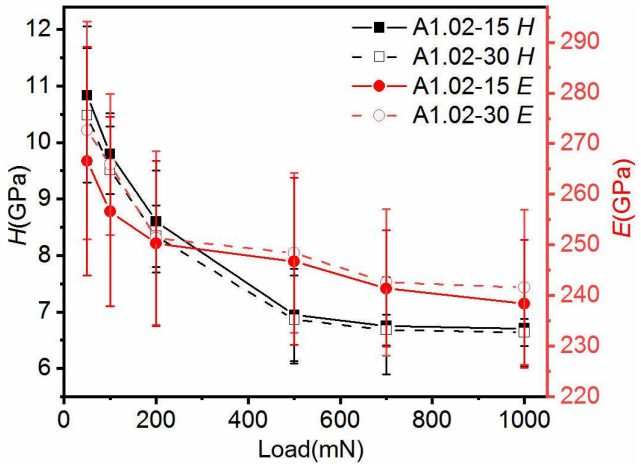

Fig.8 The hardness (*H*) and elastic modulus (*E*) at different loads (mN) via Fischer Indentation.

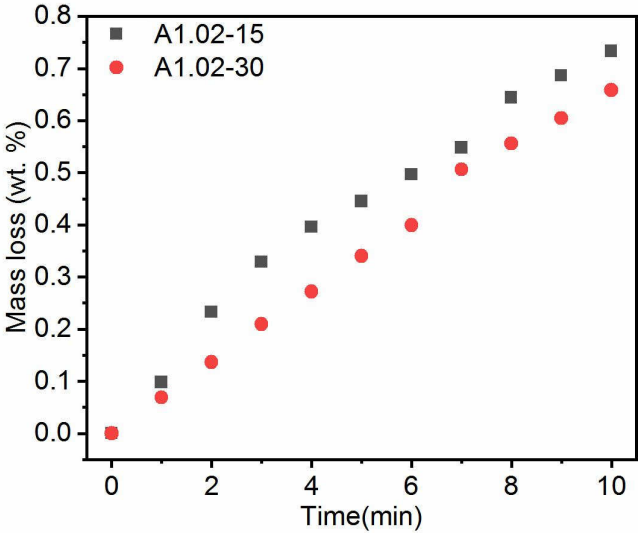

Fig.9 Mass loss of A1.02-15 and A1.02-30 as a function of sandblasting time.

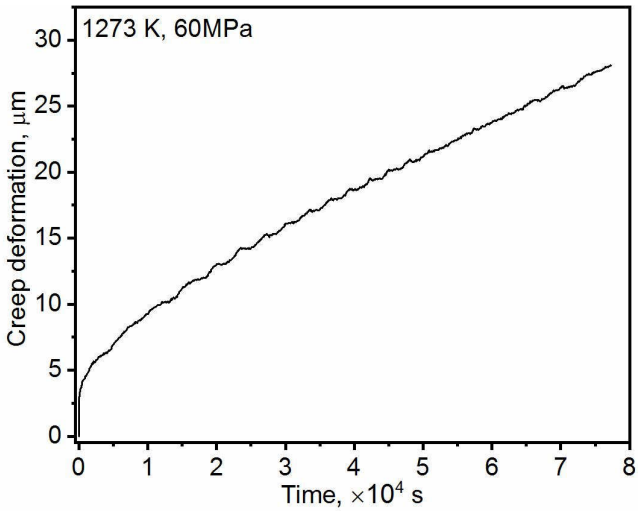

Fig.10 Example of the creep deformation of A1.02-15 at 1000 °C under 60 MPa.

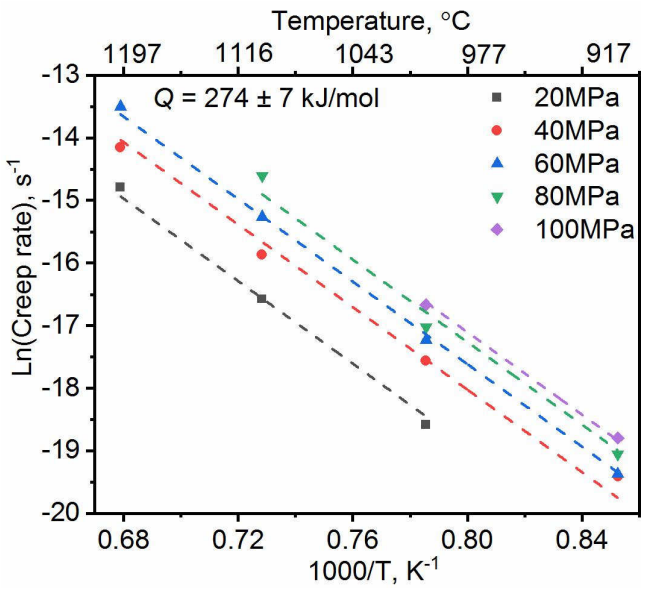

Fig.11 Arrhenius plot of the creep rates of A1.02-15 for applied the stresses from 20 MPa to 100 MPa as a function of inverse temperature.

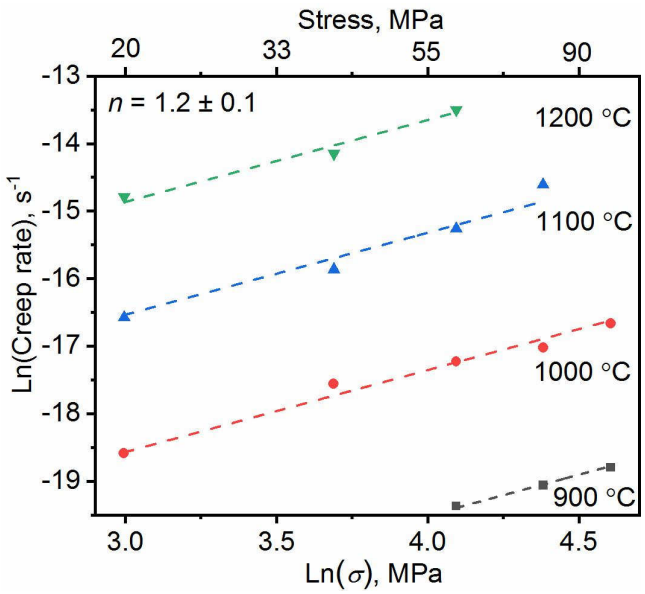

Fig.12 The ln-ln plot of creep rate as a function of applied compressive stress during the creep test for A1.02-15 in the temperature range of 900-1200 °C.

.

Table 1 The conditions of the compressive creep test on A1.02-15

Material	Geometry(mm^2)	Temperature(℃)	Stress (MPa)			
A1.02-15	∅6×8	900	40	60	80	100
		1000	20	40	60	80	100
		1100	20	40	60	80	
		1200	20	40	60		

Table 2 The compositions and lattice parameters of bulk Ti_2AlN ceramics via Rietveld analysis

Sample	Phase	Ti_2AlN	Ti_3Al	$AlTiN_2$	$AlTi_3N$	TiAl
	SG	P63/mmc	P63/mmc	Fm-3m	Pm-3m	P4/mmm
	ICSD	184882	58188	608638	52642	58187
A1-15	Wt%	96	2	1	1	
	a[Å]	2.987	5.763	4.23	4.110	
	c[Å]	13.643	4.632			
A1.01-15	Wt%	100				
	a[Å]	2.988				
	c[Å]	13.640				
A1.02-15	Wt%	100				
	a[Å]	2.987				
	c[Å]	13.644				
A1.03-15	Wt%	93	3		1	3
	a[Å]	2.987	5.753		4.112	2.823
	c[Å]	13.636	4.635			4.062
A1.02-30	Wt%	100				
	a[Å]	2.987				
	c[Å]	13.645				

Table 3 The summary of the reported literature about the creep test on MAX phase ceramics

		Grain size (μm)	T (°C)	σ (MPa)	Q (kJ/mol)	n	Creep mechanism	Reference
Ti_3SiC_2		3-5	1000-1200	10-100	445±10	1.5 ±0.1	Plastic deformation	45
Ti_2AlC	Tensile creep	14±8	1000-1150	10-40	362±88	2.5±0.3	Dislocation creep	48
Ti_3AlC_2		4.9-12.5	900-1000	45-210		2	Grain boundary sliding	49
Ti_3SiC_2		3-5	1000-1200	10-100	768±20	1.9±0.4	Dislocation creep	47
Cr_2AlC	Compressive creep	9	800-1200	1-12	429±13	2.7±0.2	Dislocation motion and/or the grain boundary sliding	50
Ti_2AlN		10±5	900-1200	20-100	274±7	1.2±0.1	Dislocation motion and/or the grain boundary sliding	Current work